Available online at www.sciencedirect.com
SCIENCE DIRECT
Solid State Ionics 177 (2006) 833–842
SOLID STATE IONICS
www.elsevier.com/locate/ssi

Phase stability and oxygen non-stoichiometry of $SrCo_{0.8}Fe_{0.2}O_{3-\delta}$ measured by in situ neutron diffraction

Steven McIntosh [a,1], Jaap F. Vente [b], Wim G. Haije [b], Dave H.A. Blank [a], Henny J.M. Bouwmeester [a,*]

[a] *Inorganic Material Science, Department of Science and Technology and MESA+ Institute for Nanotechnology, University of Twente, 7500 AE Enschede, Netherlands*
[b] *Energy Research Centre of the Netherlands, 1755 ZG Petten, Netherlands*

Received 7 December 2005; received in revised form 26 January 2006; accepted 7 February 2006

Abstract

The phase stability, oxygen stoichiometry and expansion properties of $SrCo_{0.8}Fe_{0.2}O_{3-\delta}$ (SCF) were determined by in situ neutron diffraction between 873 and 1173 K and oxygen partial pressures of 5×10^{-4} to 1 atm. At a pO_2 of 1 atm, SCF adopts a cubic perovskite structure, space group $Pm\bar{3}m$, across the whole temperature range investigated. At a pO_2 of 10^{-1} atm, a two-phase region exists below 922 K, where the cubic perovskite phase coexists with a vacancy ordered brownmillerite phase, $Sr_2Co_{1.6}Fe_{0.4}O_5$, space group *Icmm*. A pure brownmillerite phase is present at pO_2 of 10^{-2} and 5×10^{-4} atm below 1020 K. Above 1020 K, the brownmillerite phase transforms to cubic perovskite through a two-phase region with no brownmillerite structure observed above 1064 K. Large distortion of the BO_6 (B=Co, Fe) octahedra is present in the brownmillerite structure with apical bond lengths of 2.2974(4) Å and equatorial bond lengths of 1.9737(3) Å at 1021 K and a pO_2 of 10^{-2} atm. SCF is highly oxygen deficient with a maximum oxygen stoichiometry, $3-\delta$, measured in this study of 2.58(2) at 873 K and a pO_2 of 1 atm and a minimum of 2.33(2) at 1173 K and a pO_2 of 5×10^{-4} atm. Significant differences in lattice volume and expansion behavior between the brownmillerite and cubic perovskite phases suggest potential difficulties in thermal cycling of $SrCo_{0.8}Fe_{0.2}O_{3-\delta}$ membranes.

Keywords: Neutron diffraction; Oxygen non-stoichiometry; Chemical expansion; Brownmillerite–perovskite phase transition; Membranes; $SrCo_{0.8}Fe_{0.2}O_{3-\delta}$

1. Introduction

Among novel technologies under development as cost-effective alternatives to conventional oxygen production methods, mixed ionic–electronic conducting ceramic membranes offer great promise. These oxygen-transport membranes (OTM) selectively separate oxygen from an air supply, or other source, at elevated temperature under an oxygen chemical potential gradient. The materials for this application must exhibit high ionic and electronic conductivities between oxygen partial pressures, pO_2, of 10^{-5} to 1 atm at temperatures between 1000 and 1300 K. The crystal structure and composition of the chosen material are important parameters influencing anion and electron transport, surface kinetics and mechanical properties. To ensure constant long-term performance, the material should maintain structural, chemical and mechanical stability.

Perovskite oxides with composition $La_{1-x}Sr_xFe_{1-y}Co_yO_{3-\delta}$ are of particular interest for this application [1]. Within this series, $SrCo_{0.8}Fe_{0.2}O_{3-\delta}$ (SCF) has received considerable attention due to its high ionic and electronic conductivity [1] and, consequently, high oxygen flux [2,3]. Oxygen transport in these materials occurs via a vacancy hopping mechanism among equivalent oxygen sites. The oxygen sites are located around Fe/Co-cations with octahedral coordination in the cubic perovskite structure. However, a transition to the vacancy ordered brownmillerite structure, $Sr_2Co_{1.6}Fe_{0.4}O_5$, has been shown to occur in SCF [2–7] below a pO_2 of 0.1 atm and temperature of 1020 K. The brownmillerite structure consists of

* Corresponding author. Tel.: +31 53 4892202; fax: +31 53 4894683.
E-mail address: h.j.m.bouwmeester@tnw.utwente.nl (H.J.M. Bouwmeester).
[1] Current address: Department of Chemical Engineering, University of Virginia, Charlottesville, VA 22904-4741, U.S.A.

0167-2738/$ - see front matter © 2006 Elsevier B.V. All rights reserved.
doi:10.1016/j.ssi.2006.02.017

alternating layers of octahedrally and tetrahedrally coordinated Fe/Co-cations. Although the concentration of oxygen vacancies in the brownmillerite structure is high, oxygen transport rates are reduced as the vacancies are locked in the tetrahedral layers.

The phase diagram and oxygen stoichiometry of SCF has previously been examined using thermo-gravimetric analysis (TGA) and high temperature X-ray diffraction (HTXRD) [4,5]. In addition, Harrison et al. [6] utilized room temperature neutron diffraction to determine the oxygen non-stoichiometry and structure of the cubic perovskite and brownmillerite phases of SCF samples cooled under controlled pO_2 [6]. Li et al. [8] examined the stability of $SrCo_{0.8}Fe_{0.2}O_{3-\delta}$ membranes at 1173 K. They found that below pO_2 of $\sim 10^{-14}$ atm, the cubic perovskite phase decomposes to a three-phase mixture consisting of two Ruddlesden–Popper phases, $Sr_{n+1}(Fe, Co)_nO_{(3n+1-\delta)}$ with $n=2$ and 3 and CoO with the rocksalt structure. Measurements on membranes suggested a shallow oxygen stoichiometry profile across the membrane with lattice parameters close to that in air.

The oxygen stoichiometry of perovskite oxides is typically determined by controlled atmosphere thermo-gravimetric analysis (TGA) [4,9,10] or coulometric titration [11,12]. Both of these techniques require determination of the oxygen stoichiometry of the starting material by other methods, typically reduction in hydrogen or iodometric titration. The high temperature oxygen stoichiometry is then calculated from changes relative to this state. In contrast to this, the oxygen stoichiometry of each data point in powder neutron diffraction is determined independently with no requirement for sample calibration. Indeed, in situ powder neutron diffraction enables the simultaneous and absolute measurement of the oxygen stoichiometry, crystal structure, and, in the case when two or more phases are present, the relative abundance of the phases. These measurements are made as a function of pO_2 and temperature in the range of interest to application. We have previously used this technique to study the oxygen non-stoichiometry and chemical expansion behavior of the related material $Ba_{0.5}Sr_{0.5}Co_{0.8}Fe_{0.2}O_{3-\delta}$ (BSCF) [13]. The aim of this study is to determine the phase stability and oxygen non-stoichiometry of SCF in the pO_2 and temperature operational window of oxygen separation membranes, 10^{-5} to 1 atm and 873 to 1173 K.

2. Experimental

Phase pure commercial $SrCo_{0.8}Fe_{0.2}O_{3-\delta}$ (SCF) powder (Praxair specialty ceramics, Woodinville, WA, USA) was sintered at 1373 K for 10 h before cooling at 1 K/min to room temperature. The powder was then sieved to a particle size between 38 and 200 μm. A small particle size is desirable to facilitate rapid equilibration. Neutron diffraction measurements were carried out on the GEM beam line at the ISIS facility, Rutherford Appleton Laboratories, Chilton, UK. Full details of the experimental procedure and sample holder used have been reported elsewhere [13]. A quartz sample holder was designed which allowed powder samples, ~1.5 g, to be continually flushed with gas calibrated to have an oxygen partial pressure ranging from 10^{-5} to 1 atm (CK Gas Products Ltd., Hook, UK). The outlet pO_2 was continually monitored by a Nernstian sensor (Systech Instruments, Oxford, UK).

Data was collected on banks 3, 4, 5 and 6 of the GEM detector array, with *d*-spacing ranges of 0.5–1.85, 0.54–2.705, 0.74–4.1 and 1.3–7.15 Å respectively. Diffraction patterns were collected during slow heating ramps, 1.33 K/min, between 873 and 1273 K, while continually flushing the sample with the calibrated gas mixture and monitoring the outlet pO_2. The data sets are referred to in the following by this constant outlet pO_2. The measurement time for each diffraction pattern was dependent on the intensity of the incoming beam and resulted in a temperature spread between 5 and 10 K for each measurement. In the following, data is plotted against the final measurement temperature. The measurements were made in descending pO_2 starting at 1 atm. Before measurements at pO_2 of less than 0.1 atm, the sample was oxidized at 1173 K and cooled to 873 K in 0.1 atm of oxygen. This was to ensure oxidation of the sample at low temperatures.

Equilibration of the sample with the gas-phase was rapid at 1, 10^{-1} and 10^{-2} atm of oxygen, similar to that previously reported for $Ba_{0.5}Sr_{0.5}Co_{0.8}Fe_{0.2}O_{3-\delta}$ (BSCF) [13]. As with BSCF, oxygen release from the sample as the temperature was increased hindered measurements at the lowest pO_2. As such the measurements for a pO_2 of 5×10^{-4} atm were performed by feeding a gas with pO_2 of 10^{-5} atm. The temperature ramp rate was decreased to 0.25 K/min to control the outlet pO_2, and therefore sample equilibrium, between 4×10^{-4} and 5×10^{-4} atm throughout the temperature ramp. The decreased temperature ramp enabled increased counting time per measurement and resulted in reduced estimated standard deviations of the structural refinements for these data sets.

Rietveld [14] refinements were carried out using the GSAS package [15]. An initial fit obtained at room temperature was used as the starting point for the first high temperature measurement, 873 K in 1 atm of oxygen. Structural refinements were performed sequentially using the structure obtained from the previous refinement as the starting point for

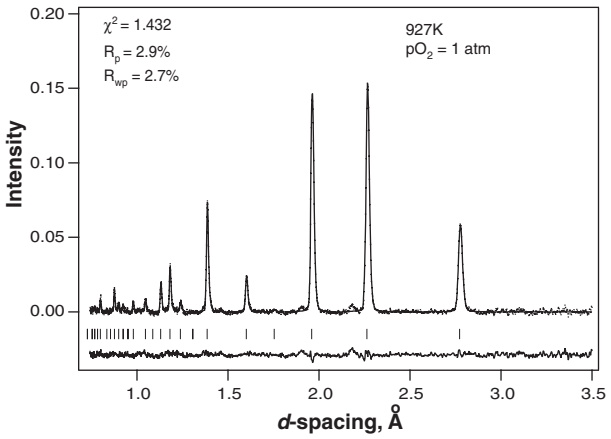

Fig. 1. Observed (dots), calculated (top line) and difference (bottom line) powder neutron diffraction patterns of SCF at 927 K and a pO_2 of 1 atm. Vertical lines indicate the peak positions for the cubic perovskite $Pm\bar{3}m$ (#221) space group.

Table 1
Refined parameters of the crystal structure of $SrCo_{0.8}Fe_{0.2}O_{2.53}$ at 927 K in $pO_2=1$ atm

Atom	Site	x	y	z	Occupancy	Thermal parameters ($Å^2$) *100		
						U_{ISO}	U_{11}	U_{22}
Sr	1b	0.5	0.5	0.5	1	2.69 (5)	–	–
Co/Fe	1a	0	0	0	1	2.42 (6)	–	–
O	3c	0.5	0	0	0.843 (3)	–	2.94 (9)	5.07 (6)

Space group $Pm\bar{3}m$ (#221), $a=3.92125(3)$Å; $V=60.2939(4)Å^3$, $\rho_c=5.134$ g/cm^3.

the current. The refined structural parameters for the cubic perovskite structure, space group $Pm\bar{3}m$, were the lattice parameter, isotropic thermal parameters for the A and B cations, the anisotropic thermal parameters for the O anion and fractional occupancy of oxygen. No correlations larger than 0.5 between this fractional occupancy and any of the other refined parameters were observed. The refined structural parameters for the orthorhombic brownmillerite structure, space group *Icmm*, were the cell parameters, fractional coordinates for all atoms, the ratio of Co to Fe on the Co/Fe(1) and Co/Fe(2) sites, isotropic thermal parameters on the A-site and Co/Fe(2) site and anisotropic thermal parameters on all other sites. The oxygen stoichiometry was fixed at 2.5. Attempts to refine this value led to scatter within one estimated standard deviation, 0.02, of 2.5 with no improvement in the quality of fit parameters.

For both structures, the total occupancy of the cation sites was fixed according to the known chemical composition while the thermal parameters of atoms on equivalent sites were constrained to be the same. Two-phase refinements were carried out using the above parameters for each phase with the addition of the relative fraction of the two phases. Further refined parameters are the scale factors and σ^{-1} profile parameters in a W.I.F. David function were refined for each pattern in both structures. Shifted Chebyschev functions with 24, 28, 34 and 36 terms were required to accurately describe the background for the cubic structure and 30, 30, 34, 34 for the brownmillerite structure for GEM banks 3, 4, 5, and 6 respectively. The coefficients of these Chebyschev functions were refined. Estimated standard deviations on the reported values for lattice parameter and oxygen stoichiometry are derived from the least square fit. For the lattice parameters, these were smaller than the symbols used in the figures.

Table 2
Rietveld fit parameters of the crystal structure of $SrCo_{0.8}Fe_{0.2}O_{2.53}$ at 927 K in $pO_2=1$ atm

Bank	d-range (Å)	R_{WP} (%)	r_P (%)	D_W-d
3	–1.3–7.2	3.92	3.96	0.830
4	–0.75–3.50	2.67	2.92	0.512
5	–0.55–2.55	2.86	2.85	0.604
6	–0.49–1.85	2.85	2.48	0.607
Sum	0.49–7.2	2.92	3.06	

χ^2(red)=1.432 for 136 variables.
Refined parameters: 1 fractional occupancy, 1 cell parameter, 4 thermal parameters, 4 scale factors, 4 profile coefficients in a W.I.F. David function, being a convolution of the Ikeda–Carpenter and pseudo-Voigt functions, 24+28+34+36 background parameters in shifted Chebyshev functions.

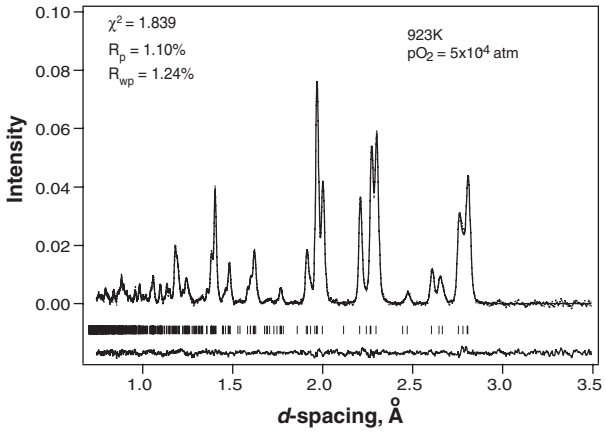

Fig. 2. Observed (dots), calculated (top line) and difference (bottom line) powder neutron diffraction patterns of SCF at 923 K and a pO_2 of 5×10^{-4} atm. Vertical lines indicate the peak positions for brownmillerite, *Icmm* (#74) space group.

3. Results

Fig. 1 shows a representative neutron diffraction pattern for the cubic phase of SCF measured at 927 K and a pO_2 of 1 atm. The R_P and R_{WP} values shown on the figure are for the individual pattern where χ^2 is the total for the structural refinement. The pattern shows the data collected for bank number 4 covering a *d*-spacing of 0.75 to 3.5 Å. The high background level, due to the quartz sample holder, is subtracted from the data. All of the peaks could be indexed using a cubic perovskite unit cell with space group $Pm\bar{3}m$. Details of the refined structural parameters are presented in Table 1. The lattice parameter and oxygen stoichiometry under these conditions were refined to 3.92125(3) and 2.52 (3) Å respectively. The weak reflections at *d*-spacings of 1.9 and 2.2 Å are attributed to the experimental apparatus. They are present in the diffraction patterns of both the perovskite and brownmillerite phases and also in the patterns recorded for BSCF using the same setup [13]. Quality of fit parameters for this pattern are presented in Table 2. The fit quality was comparable for all of the data presented in this manuscript.

Table 3
Refined parameters of the crystal structure of $Sr_2Co_{1.6}Fe_{0.4}O_5$ at 923 K in $pO_2=5\times10^{-4}$ atm

Atom	Site	x	y	z	Occupancy
Sr	8h	0.0098(4)	0.1119(1)	0.5	1
Co/Fe(1)	4a	0	0	0	0.716/0.284(5)
Co/Fe(2)	8i	−0.066(1)	0.25	−0.037(3)	0.442/0.058(2)
O(1)	8g	0.25	−0.0049(2)	0.25	1
O(2)	8h	0.0386(7)	0.1430(2)	0	1
O(3)	8i	0.8674(8)	0.25	0.6245(8)	0.5

Space group *Icmm* (#74), $a=5.61007(8)$Å, $b=15.9858(2)$Å, $c=5.50854(8)$Å; $V=494.01(1)Å^3$.

Table 4
Anisotropic thermal factors of the crystal structure of $Sr_2Co_{1.6}Fe_{0.4}O_5$ at 923 K in $pO_2 = 5 \times 10^{-4}$ atm

Atom	Thermal factors, Å^2*100					
	U_{ISO}	U_{11}	U_{22}	U_{33}	U_{12}	U_{13}
Sr	1.75(3)	–	–	–	–	–
Co/Fe(1)	–	1.2(2)	7.0(3)	1.9(2)	−0.0(2)	–
Co/Fe(2)	0.9(2)	–	–	–	–	–
O(1)	–	2.4(1)	2.3(1)	1.81(7)	–	0.05(9)
O(2)	–	3.5(2)	2.8(1)	3.8(1)	1.3(1)	–
O(3)	–	2.9(2)	2.0(2)	2.0(2)	–	−1.3(1)

Fig. 2 shows a representative neutron diffraction pattern for the brownmillerite phase of SCF measured at 923 K and a pO_2 of 5×10^{-4} atm. As with Fig. 1, the R_P and R_{WP} values shown on the figure are for the individual pattern where χ^2 is the total for the structural refinement. The pattern shows the data collected for bank number 4 covering a *d*-spacing of 0.75 to 3.5 Å with the background subtracted. All of the peaks could be indexed on an orthorhombic brownmillerite unit cell, $Sr_2Co_{1.6}Fe_{0.4}O_5$, with space group *Icmm*. Details of the refined structural parameters are presented in Tables 3–5, and selected bond lengths and angles are presented in Table 6. The lattice parameters under these conditions were refined to $a = 5.61007(8)$, $b = .9858(2)$ and $c = 5.50854(8)$ Å. No weak super lattice reflections, analogous to those reported by Harrison et al. [6], were observed.

The phase diagram of SCF in the T–pO_2 space investigated consists of three regions; cubic perovskite, oxygen vacancy ordered brownmillerite and a two-phase transition region. The lattice parameters for the cubic perovskite region are shown in Fig. 3. At a pO_2 of 1 atm, the cubic perovskite phase is stable over the whole temperature range investigated. Two phase regions exist between 873 and 925 K at a pO_2 of 10^{-1} atm and between 1021 and 1058 K at a pO_2 of 10^{-2} atm. The extent of the two-phase region at a pO_2 of 5×10^{-4} atm could not be fully resolved due to a neutron beam outage, but is estimated to exist between 1020 and 1060 K. The edges of the two-phase regions were determined as the point at which two-phase refinements lead to poorer quality structural refinements when compared to single phase refinements. The trends in refined phase fractions are in agreement with this criterion. At lower temperatures the SCF exists in the vacancy ordered brownmillerite phase.

Table 5
Fit parameters for the structural refinement of $Sr_2Co_{1.6}Fe_{0.4}O_5$ at 923 K in $pO_2 = 5 \times 10^{-4}$ atm

Bank	*d*-range (Å)	R_{WP} (%)	r_P (%)	$D_W - d$
3	1.3–7.2	1.99	1.96	0.679
4	0.75–3.50	1.26	1.11	0.543
5	0.55–2.55	1.29	1.19	0.609
6	0.49–1.85	1.73	1.32	0.435
totals	0.49–7.2	1.48	1.41	

χ^2(red) = 1.906 for 167 variables. No serial correlation in fit at 90% confidence for $1.973 < D_W - d < 2.027$.
Refined parameters: 14 atomic positions, 2 fractional occupancy, 3 cell parameters, 12 thermal parameters, 4 scale factors, 4 profile coefficients in function 2 W.I.F. David function, being a convolution of the Ikeda–Carpenter and pseudo-Voigt functions, 30+30+34+34 background parameters shifted Chebyshev function.

Table 6
Selected bond length (Å) and angles (°) of $Sr_2Co_{1.6}Fe_{0.4}O_5$ at 923 K in $pO_2 = 5 \times 10^{-4}$ atm

Sr–O(1) × 2	2.684(2)	Co/Fe(1)–O(1) × 4	1.9672(1)
Sr–O(1) × 2	2.635(2)	Co/Fe(1)–O(2) × 2	2.296(2)
Sr–O(2) × 2	2.8034(4)	Co/Fe(2)–O(2) × 2	1.818(3)
Sr–O(2)	2.583(3)	Co/Fe(2)–O(3)	1.758(8)
Sr–O(3) × 2	2.445(2)	Co/Fe(2)–O(3)	1.911(9)
O(1)–Co/Fe(1)–O(1)	88.86(6)/91.13(6)	Co/Fe(1)–O(1)–Co/Fe(1)	175.4(1)
O(1)–Co/Fe(1)–O(2)	88.5(1)/91.5(1)	Co/Fe(1)–O(2)–Co/Fe(2)	155.1(3)
		Co/Fe(2)–O(2)–Co/Fe(2)	12.9(1)
O(2)–Co/Fe(2)–O(2)	140.4(5)		
O(2)–Co/Fe(2)–O(3)	103.3(4)/100.1(6)		
O(3)–Co/Fe(2)–O(3)	106.2(5)		

Fig. 4a and b shows the polyhedral and 50% probability thermal ellipsoidal representations of the structure detailed in Tables 3 and 4. In the interests of clarity, the polyhedra and ellipsoids are shown in the fully ordered brownmillerite structure, space group *Ibm2*. The refined space group, *Icmm*, represents incomplete ordering of the brownmillerite structure [6,16]. In this structure, the tetrahedral layer is disordered with splitting of the Co/Fe(2) and O(3) sites allowing two possible orientations of each tetrahedron. Fig. 4c shows a 50% probability thermal ellipsoid representation of the split Co/Fe (2) and O(3) positions and corresponding bonds and orientations of a tetrahedron in the *Icmm* space group. The unoccupied Co/Fe(2) and O(3) positions and bonds for each orientation are shown partially shaded.

Two-phase structural refinements were performed in the transition regions of the phase diagram. Fig. 5 shows the lattice parameters and percentage brownmillerite phase for a pO_2 of 10^{-1} atm between 873 and 1173 K. The lattice parameters of the brownmillerite phase are scaled to $a/\sqrt{2}$, $b/4$, and $c/\sqrt{2}$ to aid comparison with the cubic unit cell. No pure brownmillerite region was observed in this pO_2 and temperature range.

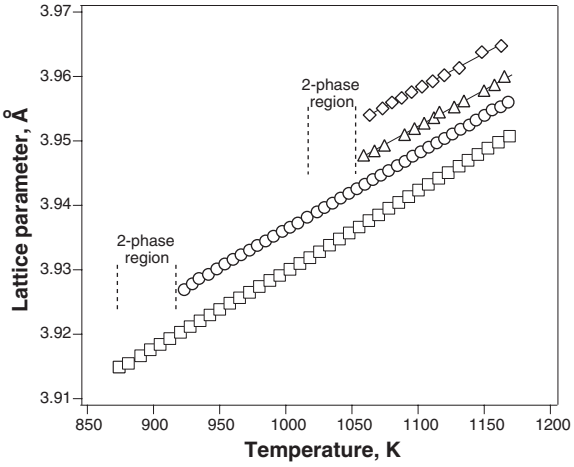

Fig. 3. Lattice parameter vs. temperature for the cubic perovskite phase $SrCo_{0.8}Fe_{0.2}O_{3-\delta}$ $pO_2 = 1$ (□), 10^{-1} (○), 10^{-2} (△) and 5×10^{-4} (◇) atm.

Expansion of both phases in the two-phase region is apparent with the lattice parameters increasing as the temperature is increased. In addition, the fraction of brownmillerite phase decreases with increasing temperature. There is a rapid shift in the brownmillerite lattice parameters towards that of the cubic phase at the final point in the two phase region, 916 K, 14.93(6) wt.% brownmillerite. This data proves the presence of the two-phase region suggested by Liu et al. [4] and Grunbaum et al. [5] on the basis of TGA studies.

The brownmillerite to perovskite transition is shifted to higher temperatures at lower pO_2. Fig. 6 shows the lattice parameters and percentage brownmillerite phase for a pO_2 of 10^{-2} atm between 873 and 1173 K. Below 1021 K SCF exists as a pure brownmillerite phase. As the temperature increases above 1021 K, the weight percentage of brownmillerite smoothly decreases, reaching zero at 1064 K where only the cubic phase is present. As with the data at higher pO_2, the lattice parameters of the brownmillerite phase shift towards those of the cubic unit cell at the high temperature edge of the two-phase region.

The change in lattice volume occurring upon phase transition is shown in Fig. 7a. The cell volume of the brownmillerite phase is significantly larger than that of the coexisting cubic phase in the two-phase region, 1.265(2)% at 1021 K. The bond lengths within the octahedra, shown in Fig. 7b, demonstrate the large distortion present in the brownmillerite phase octahedra. The Co/Fe(1)–O(2) apical bond is significantly longer than the Co/Fe(1)–O(1) equatorial bond. At the upper temperature edge of

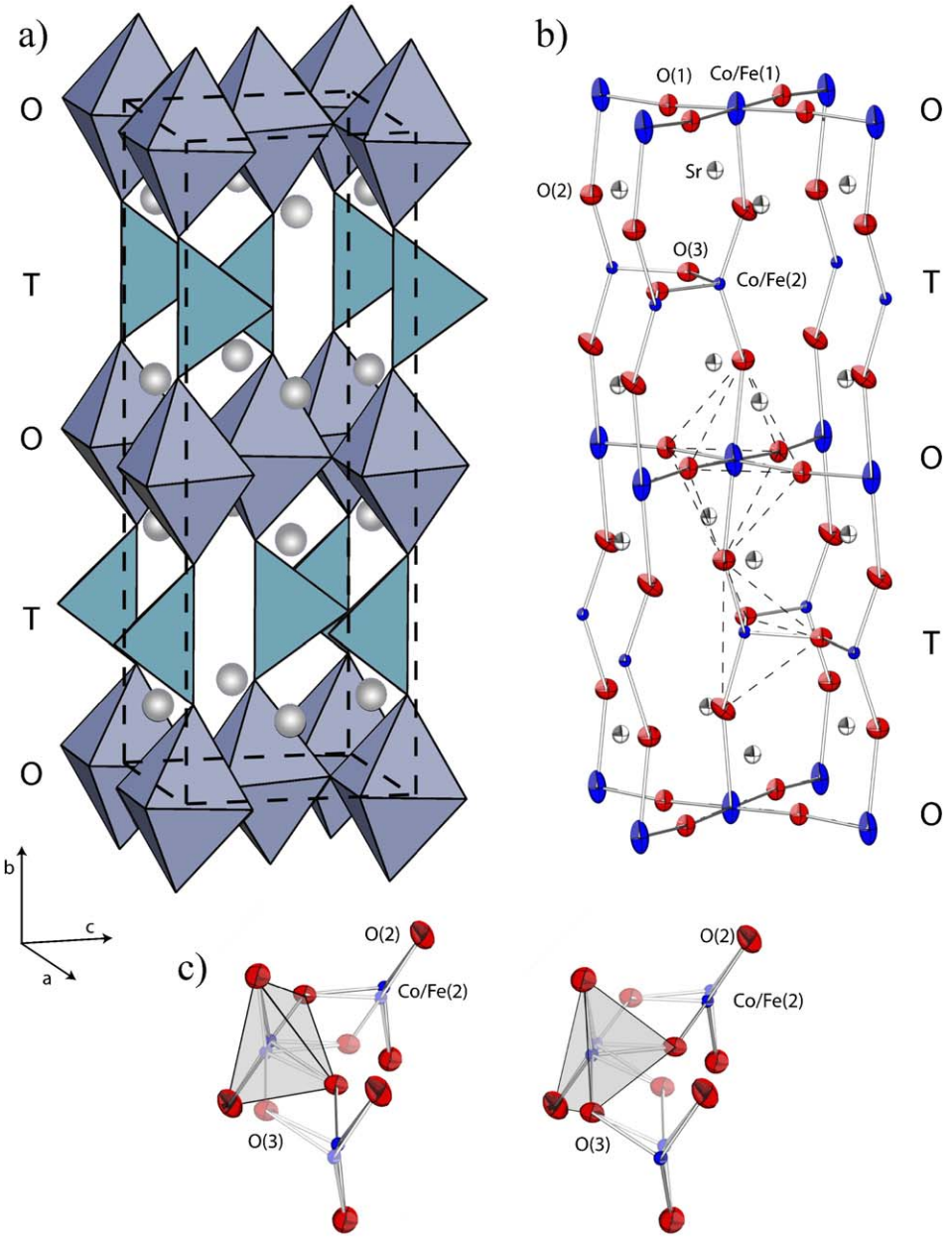

Fig. 4. Crystal structure of the $SrCo_{1.6}Fe_{0.4}O_5$ brownmillerite phase shown in Fig. 2 and detailed in Tables 3, 4, 5 and 6. a) Co/Fe–O polyhedra, b) thermal ellipsoids and c) detail, rotated out of the page, showing the two possible tetrahedron orientations across the split O(3) and Co/Fe(2) positions in the *Icmm* (#74) space group.

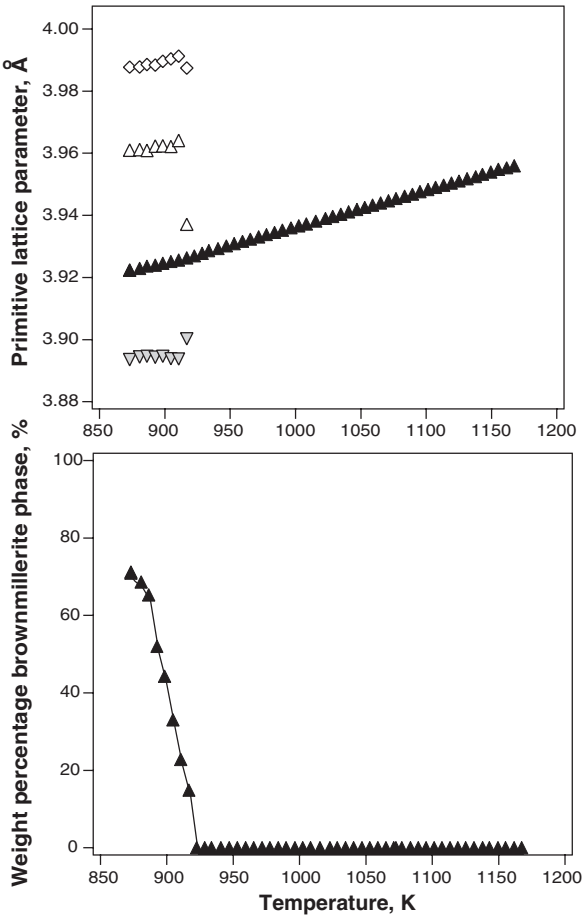

Fig. 5. a) Lattice parameters, $a/\sqrt{2}$ (△), $b/4$ (◊), and $c/\sqrt{2}$ (▼) for the brownmillerite phase and a (▲) for the cubic perovskite, and b) percentage brownmillerite phase vs. temperature for pO_2 of 10^{-1} atm.

the two-phase region this elongated bond decreases in length towards the octahedral bond length in the cubic phase. The equatorial bond is of similar length, and shows similar temperature dependence, to the octahedral bond within the cubic phase.

Fig. 8 shows the rapid transformation of the perovskite phase into the brownmillerite phase upon cooling the sample. The sample reaches 1173 K at a pO_2 of 10^{-2} atm and is cooled to 873 K within the time-span of one measurement, 6 min. The SCF structure is completely converted from 100% cubic perovskite to 100% vacancy ordered brownmillerite within this short time. The brownmillerite lattice parameters reach a plateau within 10 min of reaching 873 K. This demonstrates both the rapid equilibration of the sample in our system and the difficulty in quenching samples from high temperature.

As previously mentioned, the two-phase region at a pO_2 of 5×10^{-4} atm was obscured due to a beam outage. The lattice parameters refined from the data collected are presented in Fig. 9. A comparison of this set with that at a pO_2 of 10^{-2} atm, Fig. 6, suggests that the two-phase region would span the entire period of beam outage, however, this cannot be fully ascertained.

Finally, Fig. 10 shows the oxygen stoichiometry of the perovskite phase of SCF determined from the structural refinements. Refinements of the oxygen content in the brownmillerite phase did not lead to any improvement in the quality of fit parameters and introduced scatter around the ideal value of 2.5. The oxygen stoichiometry in the brownmillerite region was set to 2.5 in the refinements and is, therefore, represented by a line. In addition, attempts to refine the oxygen content of the cubic perovskite phase in the two-phase region led to convergence instabilities; the oxygen content was therefore fixed at 2.5 for the cubic perovskite in the two-phase regions.

4. Discussion

The use of in situ powder neutron diffraction techniques allows the phase transition from the brownmillerite to perovskite phase to be studied in detail. This transition occurs through a significant two-phase region. Within which, the brownmillerite phase fraction decreases smoothly with increasing temperature. Previous studies report the stability regions of the brownmillerite determined by TGA or XRD [4,5]. These techniques allow the limits of the brownmillerite stability region to be determined, but not the behavior within the transition region itself. A pure brownmillerite phase exists below 1020 K at pO_2 of 10^{-2} and 5×10^{-4} atm. However, at the higher pO_2 of

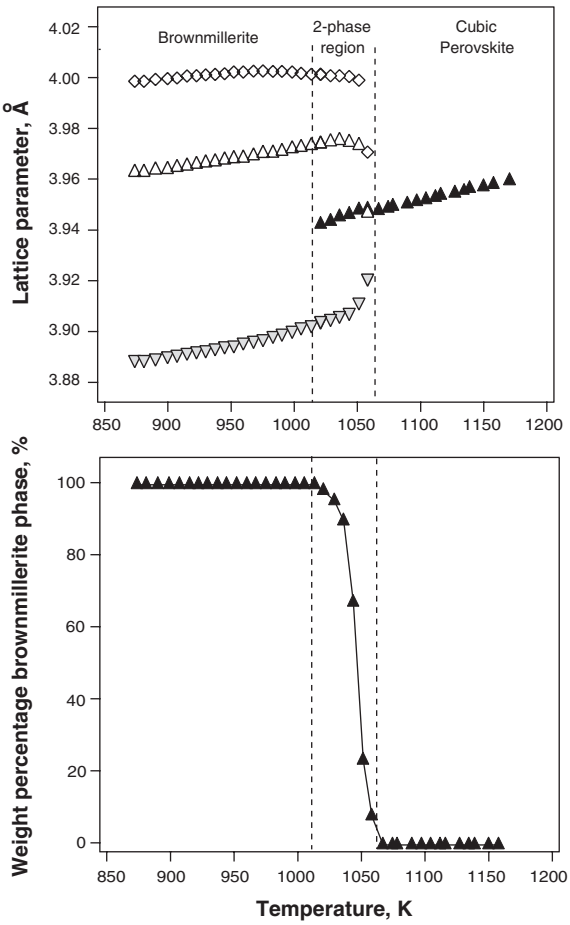

Fig. 6. a) Lattice parameters $a/\sqrt{2}$ (△), $b/4$ (◊), and $c/\sqrt{2}$ (▼) for the brownmillerite phase and a (▲) for the cubic perovskite, and b) percentage brownmillerite phase vs. temperature for a pO_2 of 10^{-2} atm.

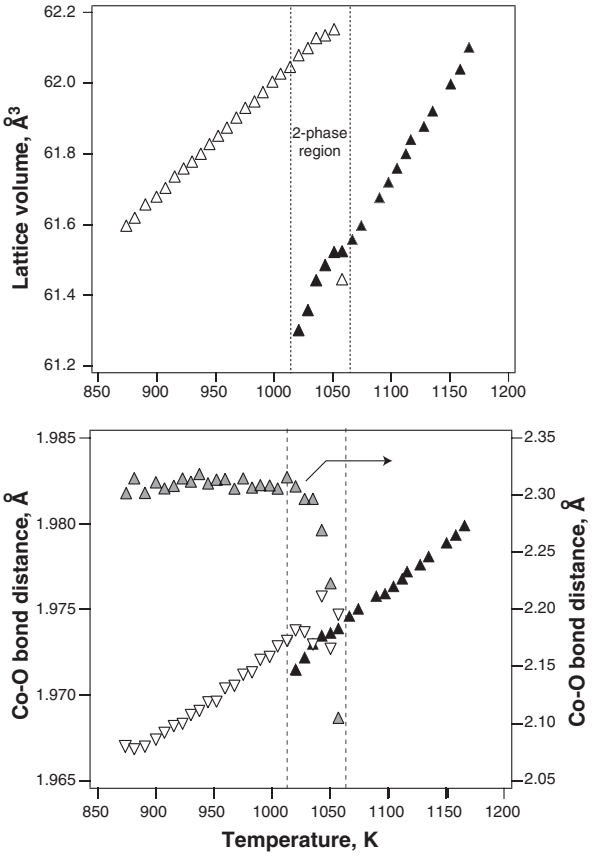

Fig. 7. a) Lattice volume for the brownmillerite, $a/\sqrt{2}*b/4*c/\sqrt{2}$ (△), and cubic perovskite phases, a^3 (▲), versus temperature for a pO_2 of 10^{-2} atm. b) Co/Fe–O octahedral bond distances in the brownmillerite, Co/Fe(1)–O(1) (▽) and Co/Fe(1)–O(2) (), and cubic perovskite (▲) phases versus temperature.

0.1 atm, the brownmillerite phase is present in equilibrium with the perovskite phase between 873 and 925 K. The transition to the pure cubic perovskite phase with increasing temperature is complete by 922 K at a pO_2 of 10^{-1} atm and by 1065 K at pO_2 of 10^{-2} and 5×10^{-4} atm, in accordance with [4,5].

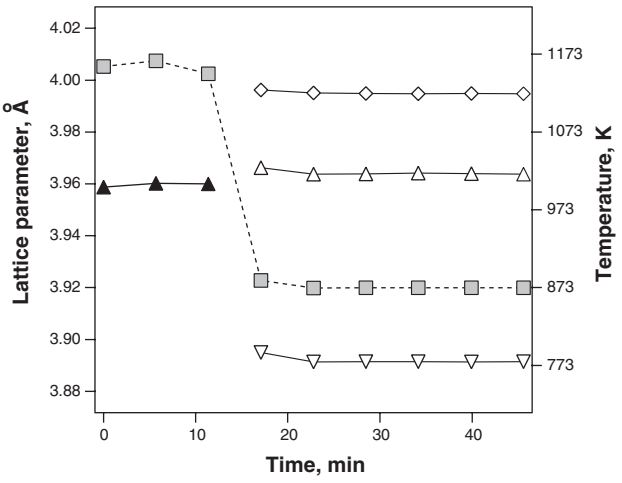

Fig. 8. Lattice parameters $a/\sqrt{2}$ (△), $b/4$ (◊), and $c/\sqrt{2}$ (▽) for the brownmillerite phase and a (▲) for the cubic perovskite, and temperature (■) upon cooling of the sample for a pO_2 of 10^{-2} atm.

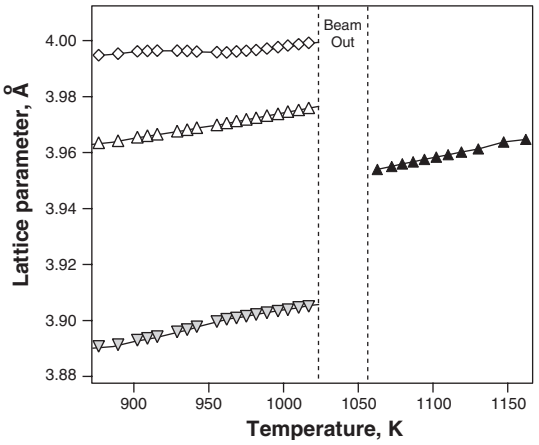

Fig. 9. a) Lattice parameters $a/\sqrt{2}$ (△), $b/4$ (◊), and $c/\sqrt{2}$ (▼) for the brownmillerite phase and a (▲) for the cubic perovskite, vs. temperature for a pO_2 of 5×10^{-4} atm.

The occurrence of this two phase region may be compared to related systems. A fully disordered perovskite phase, a brownmillerite phase and two intermediate stoichiometry intergrowth structures, $SrFeO_{2.75}$ and $SrFeO_{2.86}$ have been reported for the system $SrFeO_{3-\delta}$ [17,18] . Comparison with the Sr–Co–O system is complicated due to the formation of $Sr_6Co_5O_{15}$ [19].

The oxygen stoichiometry of the perovskite phase determined in this study is significantly lower than previously reported [4,5]. The reason for this discrepancy is not immediately apparent but may be related to difficulties in measuring the absolute stoichiometry of the starting material by, for example, reduction in hydrogen when using TGA or coulometric titration. In support of the work presented here, neutron diffraction is a sensitive and accurate technique and the quality of fit parameters obtained from our structural refinements are very good. Furthermore, refined oxygen stoichiometries for the brownmillerite phase were within one standard deviation of the ideal value, 2.5. These results prove that the appropriate scattering length for oxygen has been used. One possible reason for the disagreement in oxygen stoichiometry with literature data is a lack of equilibration of the cubic perovskite phase during our measurements. However, a lack of equilibration is expected to lead to increased oxygen stoichiometry as the sample was previously annealed in air and measurements were performed in order of increasing temperature and decreasing pO_2. In addition, short equilibration times, especially at higher values of pO_2, have been demonstrated in Fig. 8 and for our previous measurements [13].

Further substantiation of the oxygen stoichiometries determined in this study can be found in the brownmillerite–perovskite transition at a pO_2 of 10^{-1} atm. This pO_2 is close to the upper limit of brownmillerite phase stabilization [4,5] and it may be expected that the perovskite phase close to this transition point has an oxygen stoichiometry close to 2.5. Our measurements show a smooth transition from the brownmillerite phase, with ideal oxygen stoichiometry of 2.5, to a pure cubic perovskite structure with refined oxygen stoichiometry of 2.50(2) at 869 K. This internal reference provides further

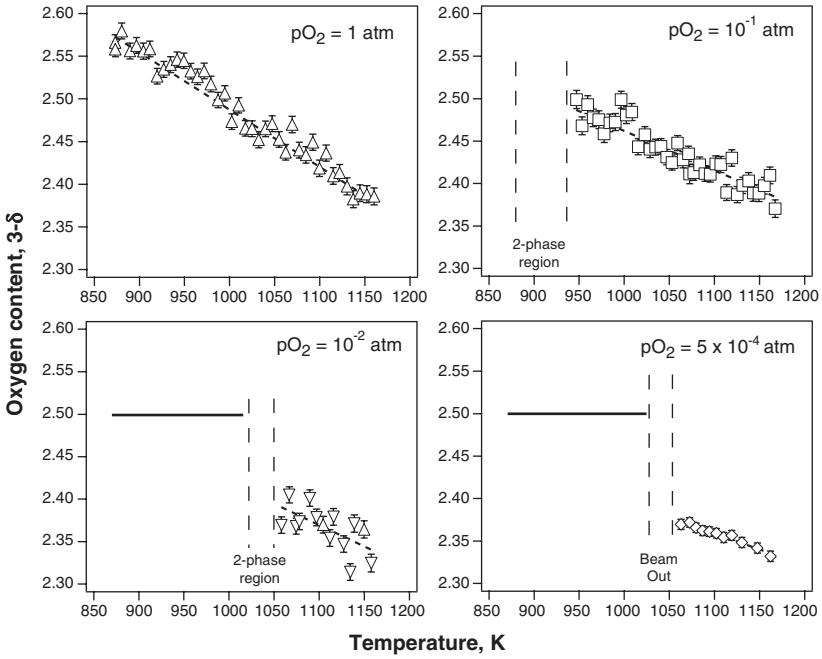

Fig. 10. Oxygen content vs. temperature for pO_2 of 1 (△), 10^{-1} (□), 10^{-2} (▽) and 5×10^{-4} (◊) atm.

evidence for the accuracy of the oxygen stoichiometries determined in this study. The significant reduction in oxygen stoichiometry upon transition to the perovskite phase at lower pO_2 is consistent with data present in the literature, although the absolute perovskite oxygen stoichiometry determined in this study is lower. The maximum oxygen stoichiometry is 2.58(2) at 873 K and a pO_2 of 1 atm with the minimum of 2.33(2) at 1173 K and a pO_2 of 5×10^{-4} atm. The oxygen stoichiometry of SCF is greater than that of BSCF determined by neutron diffraction and confirmed by thermogravimetric methods [13]. This is congruent with the higher oxygen flux through BSCF membranes reported in the literature [20,21].

The distortion of the BO_6 (B=Co, Fe) octahedra in the brownmillerite phase of SCF is pronounced. For example, at 923 K and a pO_2 of 5×10^{-4} atm, the Co/Fe(1)–O(2) apical bond is 2.296(2) Å, compared with the Co/Fe(1)–O(1) equatorial bond length of 1.9672(1) Å, as shown in Table 6. This tetragonal distortion in brownmillerite is a common feature, with the difference between apical and equatorial bonds typically around 0.20 Å [22]. As noted above, it is 0.32 Å at 923 K and a pO_2 of 5×10^{-4} atm and one may speculate as to the origin of this enhanced effect. E⊗ε Jahn–Teller distortions of the Co^{3+} octahedra that may amplify this difference are possible through a thermally excited spin state S=1, $t_{2g}^5e_g^1$ [23,24]. Similarly, large distortions, 0.4 Å, have been found for Jahn–Teller active Mn^{3+} in $Sr_2MnGaO_{3+\delta}$ quenched from 700 K [25]. Furthermore, increasing amounts of Jahn–Teller active Cu^{2+} have been shown to increase the difference between apical and equatorial bond lengths in $Ba_2In_{2-x}Cu_xO_5$ [26]. However, it should be noted that the temperature range probed in this study is significantly higher than these previous reports of cooperative Jahn–Teller distortions. Further study is required to confirm this hypothesis.

The octahedral tilting is accompanied by the anisotropic thermal motion of the O(2) and O(3) sites, shown in Fig. 4 and Table 4. The thermal motion of the cation within the octahedra is large and may suggest splitting of this site along the long Co/Fe(1)–O(2) bond vector. The splitting of the tetrahedral B cation site in the *Icmm* space group may be due to averaging over microdomains with different tetrahedral orientations or thermal motion within brownmillerite structure. The tetrahedral sites are also heavily distorted with the O(2)–Co/Fe(2)–O(2) bond angle increased to 140.4(5)°. These distortions are similar to those reported by Harrison et al. [6] for SCF at room temperature.

No significant trend in the thermal parameters of either phase could be distinguished within the accuracy of our measurements. However, a comparison between the two pure phases is useful. The anisotropic thermal parameters for brownmillerite at 923 K a pO_2 of 5×10^{-4} are listed in Table 4 and may be compared to the isotropic thermal parameter of $7.95(5)\times10^{-2}$ Å^2 for the perovskite phase at 1063 K and the same pO_2. This approximately three-fold increase in the thermal parameter is larger than predicted for the change in temperature and reflects the increased mobility and, hence, uncertainty in the location of the oxygen ions in the vacancy-disordered perovskite phase.

The brownmillerite octahedral equatorial bond length is close to that of the octahedral bond length in the cubic phase. At 1021 K and a pO_2 of 10^{-2} atm, the equatorial bond in the brownmillerite octahedra is 1.9737(3) compared to 1.9722(8) Å for the corresponding bond in the coexisting cubic phase, as shown in Fig. 7b. The longer apical bond length decreases towards that in the cubic perovskite, accompanied by a significant decrease in lattice volume, as the brownmillerite phase transforms to cubic perovskite, shown in Fig. 7.

A slight preference for Fe to reside on the octahedral site of the brownmillerite structure is observed. At a pO_2 of 10^{-2} atm, the octahedral occupancy of iron is 0.252(8) at 890 K, above the value of 0.2 expected for a random distribution of cations in the lattice. This preference for the octahedral site is consistent with the observations reported by Harrison et al. [6] for SCF and Battle et al. [27] for Sr_2CoFeO_5.

The chemical and thermal expansion coefficients of SCF may be extracted from the structural parameters and oxygen stoichiometry. The strains associated with the total, chemical and thermal expansion and total volumetric expansion, respectively, are defined as

$$\varepsilon_T = \frac{(a-a_0)}{a_0}\Big|_{pO_2=\text{constant}} \quad (1)$$

$$\varepsilon_c = \frac{(a-a_0)}{a_0}\Big|_{T=\text{constant}} \quad (2)$$

$$\varepsilon_{Th} = \frac{(a-a_0)}{a_0}\Big|_{\delta=\text{constant}} \quad (3)$$

$$v_T = \frac{(V-V_0)}{V_0}\Big|_{pO_2=\text{constant}} \quad (4)$$

where a is the lattice parameter, V is the lattice volume and a_0 and V_0 are the lattice parameter and volume at the reference state. The lattice volume is a^3 for the cubic perovskite phase and was taken as $a/\sqrt{2} \times b/4 \times c/\sqrt{2}$ for the brownmillerite phase. This allows a direct comparison between the two phases. For the total linear and volumetric expansion, the reference state was set at 873 K at the pO_2 of interest. For chemical expansion, a_0 was the lattice parameter at an oxygen stoichiometry of 2.44 and the temperature of interest. For thermal expansion, a_0 was the lattice parameter at 873 K and the δ of interest. The total, chemical and thermal expansions are defined as $\varepsilon_T/\Delta T$, $\varepsilon_c/\Delta\delta$, $\varepsilon_{Th}/\Delta T$ and $v_T/\Delta T$. The values required for these calculations were derived from linear least squares fits to the relevant data.

The expansion behavior of the cubic perovskite phase is extracted from the results presented in Fig. 3. The total expansion, shown in Fig. 3 as the change in lattice parameter as a function of temperature at constant pO_2, is 31.13(6), 29.88(6), 29.25(6) and $27.14(5)\times10^{-6}$ K^{-1} at pO_2 of 1, 10^{-1}, 10^{-2} and 5×10^{-4} atm, respectively. At constant temperature the lattice is larger at lower pO_2 due to reduction of the B cations. The chemical expansion in the region 1073 to 1173 K was determined as $0.05(1)\times10^{-6}$. The thermal expansion coefficients were determined as 15(3) and $12(3)\times10^{-6}$ K^{-1} at δ of 0.65 and 0.60, respectively. The chemical expansion is larger than previously determined for BSCF [13] and other cubic perovskite oxides [28].

The brownmillerite phase undergoes limited chemical expansion as the oxygen stoichiometry of this phase changes little with temperature or pO_2. Therefore, the total expansion of this phase is approximately equivalent to the thermal expansion. The expansion coefficients were calculated using Eq. (3) for each of the lattice parameters and are 19.21(7), 4.76(6) and $26.87(9)\times10^{-6}$ K^{-1} along the a, b and c axis respectively at a pO_2 of 10^{-1} atm. The limited expansion along the b axis is further evidenced by the small change in Co/Fe(1)–O(2) bond length shown in Fig. 7b. This may be attributed to the lower cation packing density in this direction.

At a pO_2 of 5×10^{-4} atm, the expansion coefficients increase to 22.4(1), 7.83(8) and $26.25(9)\times10^{-6}$ K^{-1} along the a, b and c axis, respectively. This increased expansion with decreasing pO_2 may be evidence for limited chemical expansion due to the formation of vacancies in the brownmillerite structure. Deviations of 0.02 from the ideal brownmillerite stoichiometry of 2.5 have been reported in the literature [5,27], however this is close to the standard deviation in refined oxygen stoichiometry, 0.02, in our experiments. As described above, it was not possible to resolve a trend in brownmillerite oxygen stoichiometry from the data presented here.

Comparison between the expansion of the cubic perovskite and brownmillerite phases is enabled by considering the total volumetric expansion. The total volumetric expansion coefficients of the pure brownmillerite phase at pO_2 of 10^{-2} and 5×10^{-4} atm are 49.9(7) and $56.3(7)\times10^{-6}$ K^{-1}, respectively. The corresponding values for the pure perovskite phase are 84.2 (1) and $81.6(1)\times10^{-6}$ K^{-1}. This large increase in volumetric expansion complicates the application of SCF membranes, especially concerning thermal cycling under pO_2 gradients where, as shown in Fig. 8, the brownmillerite phase forms under very mild conditions of temperature and pO_2.

5. Conclusions

$SrCo_{0.8}Fe_{0.2}O_{3-\delta}$ has the cubic perovskite structure with randomly distributed oxygen vacancies between 873 and 1173 K at a pO_2 of 1 atm. As the pO_2 is decreased, a vacancy ordered brownmillerite phase with space group *Icmm* appears. At a pO_2 of 10^{-1} atm, this vacancy ordered phase exists in a two-phase region with the cubic perovskite phase below 922 K. Above 922 K the structure reverts to a pure cubic perovskite phase. At pO_2 of 10^{-2} and 5×10^{-4} atm a pure brownmillerite phase exists below 1020 K with a two phase cubic perovskite–brownmillerite region between 1020 K and 1064 K. Above 1064 K, the material has the cubic perovskite structure. The octahedra in the brownmillerite phase are significantly distorted and tilted with elongated apical bond length in comparison to equatorial. As the material transforms to the cubic phase, this apical bond decreases in length to match that of the equatorial bond in the cubic perovskite. The brownmillerite phase expands anisotropically with limited expansion of the b-axis in comparison to the a and c axes. In addition, the volumetric expansion of the brownmillerite phase is less than that of the perovskite phase. These differences in expansion behavior may lead to difficulties in applying SCF as a membrane material. Furthermore, oxygen transport rates in the brownmillerite phase are reduced in comparison with the vacancy disordered cubic perovskite. At the same pO_2 and temperature, the oxygen stoichiometry of SCF is greater than that of BSCF, in agreement with the higher oxygen transport rates reported for BSCF.

Acknowledgements

Financial support for Steven McIntosh was provided by the EU Marie Curie Intra-European Fellowship EIF–515272 'OXYMEM'. Further financial support was provided by the Dutch Ministry of Economic Affairs through the EDI program administered by Senter-Novem under contract number EDI03201. We are grateful to Paolo Radaelli (ISIS) for experimental assistance.

References

[1] Y. Teraoka, H.M. Zhang, K. Okamoto, N. Yamazoe, Mater. Res. Bull. 23 (1988) 51.
[2] L. Qiu, T.H. Lee, L.-M. Liu, Y.L. Yang, A.J. Jacobson, Solid State Ionics 76 (1995) 321.
[3] H. Kruidhof, H.J.M. Bouwmeester, R.H.E. Doorn, A.J. Burggraaf, Solid State Ionics 63–65 (1993) 816.
[4] L.M. Liu, T.H. Lee, L. Qiu, Y.L. Yang, A.J. Jacobson, Mat. Res. Bull. 31 (1996) 29.
[5] N. Grunbaum, L. Mogni, F. Prado, A. Caneiro, J. Solid State Chem. 177 (2004) 2350.
[6] W.T.A. Harrison, T.H. Lee, Y.L. Yang, D.P. Scarfe, L.M. Liu, A.J. Jacobson, Mater. Res. Bull. 30 (1995) 621.
[7] F. Prado, N. Grunbaum, A. Caneiro, A. Manthiram, Solid State Ionics 167 (2004) 147.
[8] Y.P. Li, E.R. Maxey, J.W. Richardson, J. Am. Ceram. Soc. 88 (2005) 1244.
[9] J. Mizusaki, M. Yoshihiro, S. Yamauchi, K. Fueki, J. Solid State Chem. 58 (1985) 257.
[10] J. Mizusaki, Y. Mima, S. Yamauchi, K. Fueki, H. Tagawa, J. Solid State Chem. 80 (1989) 102.
[11] M.H.R. Lankhorst, H.J.M. Bouwmeester, J. Electrochem. Soc. 144 (1997) 1268.
[12] M.H.R. Lankhorst, H.J.M. Bouwmeester, J. Electrochem. Soc. 144 (1997) 1261.
[13] S. McIntosh, J.F. Vente, W.G. Haije, D.H.A. Blank, H.J.M. Bouwmeester, Chem. Mater. (in press), doi:10.1021/cm052763x.
[14] H.M. Rietveld, J. Appl. Crystallogr. 2 (1969) 65.
[15] A.C. Larson, R.B. Von Dreele, Los Alamos Natl. Lab. Rep., LAUR (2000) 86.
[16] F. Lindberg, S.Ya. Istomin, P. Berastegui, G. Svensson, S.M. Kazakov, E. V. Antipov, J. Solid State Chem. 173 (2003) 395.
[17] Y. Takeda, K. Kanno, T. Takada, O. Yamamoto, M. Takano, N. Nakayama, Y. Bando, J. Solid State Chem. 63 (1986) 237.
[18] B.C. Tofield, C. Greaves, B.E.F. Fender, Mater. Res. Bull. 10 (1975) 737.
[19] W.T.A. Harrison, S.L. Hegwood, A.J. Jacobson, Chem. Commun. (1995) 1953.
[20] J.F. Vente, W.G. Haije, Z.S. Rak, J. Memb. Sci. (in press), doi:10.1016/j.memsci.2005.09.046.
[21] Z. Shao, G. Xiong, J. Tong, H. Dong, W. Yang, Sep. Purif. Technol. 25 (2001) 419.
[22] P. Berastegui, S.-G. Eriksson, S. Hull, Mater. Res. Bull. 34 (1999) 303.
[23] C. Zobel, M. Kriener, D. Bruns, J. Baier, M. Gruninger, T. Lorenz, P. Reutler, A. Revcolevschi, Phys. Rev., B 66 (2002) 020402.
[24] G. Maris, Y. Ren, V. Volotchaev, C. Zobel, T. Lorenz, T.T.M. Palstra, Phys. Rev., B 67 (2003) 224423.
[25] A.M. Abakumov, M.G. Rozova, A.M. Alekseeva, M.L. Kovba, E.V. Antipov, O.I. Lebedev, G. Van Tendeloo, Solid State Sci. 5 (2003) 871.
[26] D.H. Gregory, M.T. Weller, J. Solid State Chem. 107 (1993) 134.
[27] P.D. Battle, T.C. Gibb, S. Nixon, J. Solid State Chem. 73 (1988) 330.
[28] A. Atkinson, T.M.G.M. Ramos, Solid State Ionics 129 (2000) 259.